Measurment of the branching fraction f_{00}: $\Upsilon(4S) \to B^0\overline{B}^0$

Bachelorarbeit an der Fakultät für Physik
der
Ludwig-Maximilians-Universität München

vorgelegt von
Philipp Zehetner
geboren in Rosenheim

München, den 24. Juli 2017

Messung des Verzweigungsverhältnisses f_{00}: $\Upsilon(4S) \to B^0\overline{B}^0$

Bachelorarbeit an der Fakultät für Physik
der
Ludwig-Maximilians-Universität München

vorgelegt von
Philipp Zehetner
geboren in Rosenheim

München, den 24. Juli 2017

Contents

Chapter 1

Motivation

1.1 Introduction

If Isospin symmetry was perfect, we would expect the two branching fractions $f_{00} = \mathcal{B}\left(\Upsilon(4\mathrm{S}) \to \mathrm{B}^0\overline{\mathrm{B}}^0\right)$ and $f_{+-} = \mathcal{B}\left(\Upsilon(4\mathrm{S}) \to \mathrm{B}^+\mathrm{B}^-\right)$ to be equal. However, isospin symmetry is only an approximate symmetry and it is broken by the small mass difference of the up and down quark and also by electromagnetic interactions. Therefore a small difference between the branching ratios f_{00} and f_{+-} can be expected. Theoretical calculations [1] and actual measurements (Table 1.2) have been made to determine the ratio

$$R^{\pm/0} = \frac{f_{+-}}{f_{00}} = 1 + \delta R^{\pm/0} \tag{1.1}$$

and will be described in the following section. However, the analysis of these measurements is partially based on the assumption of isospin symmetry. A particularly interesting measurement was made at the BABAR detector in 2008 [2], when they reported the first measurement of the branching fraction f_{00} without the assumption of isospin symmetry nor the dependence on any different branching fractions and obtained

$$f_{00} = 0.487 \pm 0.010(stat) \pm 0.008(sys). \tag{1.2}$$

A precise measurement of the branching fraction $f_{00} = \mathcal{B}\left(\Upsilon(4\mathrm{S}) \to \mathrm{B}\overline{\mathrm{B}}\right)$ interests us for two reasons: [3]

(I) The production asymmetry between charged and neutral B-mesons can be used to test theoretical calculations regarding isospin symmetry breaking. This can be used to test the standard model or otherwise to search for new physics.

(II) In high precision measurements the error on the assumption $R^{\pm/0} = 1$ is not negligible anymore. Precise knowledge of the branching ratio f_{00} helps to improve the precision of

other measurements at B-factories. The aim of this bachelor's thesis is to make a similar measurement of the branching fraction f_{00} using the data of the BELLE experiment.

1.2 Strong Isospin

Strong isospin was introduced by Werner Heisenberg [4] in 1932 after the discovery that the strong nuclear interaction doesn't differentiate between protons and neutrons. This effect can also be observed in the phenomenon of 'mirror nuclei', elements where the number of protons in element (a) matches the number of neutrons in element (b). Mirror nuclei have very similar binding energies and also share other characteristics such as spin and parity. Heisenberg's proposal was to describe protons and neutrons not as different particles, but as two different states of the same particle, called nucleon, which has isospin $I = 1/2$. The proton p and neutron n are the states that correspond to the values of the third component of isospin: $I_3 = +1/2$ for the proton and $I_3 = -1/2$ for the neutron. They can be written as $\mathrm{p} = |1/2, 1/2\rangle$ and $\mathrm{n} = |1/2, -1/2\rangle$. In the standard model, the values $\pm 1/2$ are assigned to the up and down quark u and d.

Formally isospin and angular momentum are identical, which means that exchanging every proton (up quark) for a neutron (down quark) and vice versa corresponds to a rotation in *isotopic space*. *Isospin invariance* means that physical laws are invariant under a 180° rotation in isotopic space. This symmetry is broken by the mass difference of the u and d quarks as well as by their charge difference. This symmetry breaking can be observed in the decays $\Upsilon(4\mathrm{S}) \to \mathrm{B}^0\overline{\mathrm{B}}^0$ and $\Upsilon(4\mathrm{S}) \to \mathrm{B}^+\mathrm{B}^-$. $\delta R^{\pm/0}$ can be split up into its mass and Coulomb term. Theoretical calculations [1] yield:

$$\delta R^{\pm/0} = \delta R_C^{\pm/0} + \delta R_M^{\pm/0} = \frac{\pi\alpha}{2\beta} - \frac{3\Delta m_B}{E} \tag{1.3}$$

Where α is the fine-structure constant, β the speed of the B-meson in the center-of-mass frame, $\Delta m_{\mathrm{B}\overline{\mathrm{B}}} = -0.31$ MeV is the mass difference between charged and neutral B-mesons (Table 1.1), and E is the total kinetic energy of the B-meson pair. Eq. 1.3 holds under the assumption that the $\Upsilon(4\mathrm{S})$ and both B-mesons can be treated as point-like particles and that there is no strong scattering.

Particle	$\Upsilon(4\mathrm{S})$	$\mathrm{B}^{\pm}$	B^0
M/MeV(REF)	10579.4 ± 1.2	5279.32 ± 0.14	5279.63 ± 0.15

Table 1.1: Masses of the $\Upsilon(4\mathrm{S})$ and charged and neutral B-mesons [5]

$R^{\pm/0}$			Experiment	Method
1.006	± 0.036	± 0.031	BABAR [6]	$\Upsilon(4\mathrm{S}) \to \mathrm{B\overline{B}} \to \mathrm{J/\psi K}$
1.01	± 0.03	± 0.09	BELLE [7]	$\Upsilon(4\mathrm{S}) \to \mathrm{B\overline{B}} \to dileptons$
1.058	± 0.084	± 0.136	CLEO [8]	$\Upsilon(4\mathrm{S}) \to \mathrm{B\overline{B}} \to \mathrm{D}^{*}\ell\bar{\nu}$
1.10	± 0.06	± 0.05	BABAR [9]	$\Upsilon(4\mathrm{S}) \to \mathrm{B\overline{B}} \to (\mathrm{c\bar{c}})\mathrm{K}^{*}$
1.04	± 0.07	± 0.04	CLEO [10]	$\Upsilon(4\mathrm{S}) \to \mathrm{B\overline{B}} \to \mathrm{J/\psi K}^{*}$

Table 1.2: Previous measurements of $R^{\pm/0}$

In the $\Upsilon(4\mathrm{S})$ rest-frame the speed B-meson's speed can be calculated using energy and momentum conservation:

$$M(\Upsilon(4\mathrm{S}))^2 = 4M(\mathrm{B})^2 + 4\mathbf{p}_{\mathrm{B}}^2 \tag{1.4}$$

$$\beta = \sqrt{\frac{\mathbf{p}_{\mathrm{B}}^2}{M(\mathrm{B})^2 + \mathbf{p}_{\mathrm{B}}^2}} = 0.062 \tag{1.5}$$

Inserting in Eq. 1.3 one obtains:

$$\delta R^{\pm/0} = 0.185 + 0.046 = 0.231 \tag{1.6}$$

This result is not consistent with the available experimental data in Table 1.2. The *particle data group* evaluates these measurements to $f_{00} = 1.058 \pm 0.024$ [5]. The assumption of isospin symmetry was made in these analyses, which makes them unsuitable for testing isospin symmetry [3]. However, the BABAR Collaboration has published a method that does not depend on the assumption of isospin symmetry [2]. This method is the one used in this bachelor's thesis and can be found in chapter 3

Chapter 2

The BELLE Experiment

The BELLE Experiment consists of the particle accelerator KEKB and the BELLE detector. Both shall be described briefly in this chapter.

2.1 B-factories

B-factories are experiments designed to produce B-mesons. Electrons and positrons are accelerated to a center-of-mass energy of $\sqrt{s} = 10.58$ GeV, the resonance of the $\Upsilon(4\mathrm{S})$ meson which decays in charged and neutral B-mesons. Examples are the PEP-II accelerator used at the BABAR experiment and the KEKB accelerator used for the BELLE experiment. The BELLE detector recorded a total number of $N_{\mathrm{B\overline{B}}} = (771.581 \pm 10.566) \cdot 10^6$ decays $\Upsilon(4\mathrm{S}) \to \mathrm{B\overline{B}}$.

2.2 KEKB Accelerator

The KEKB accelerator is an asymmetric electron positron collider located at the *High Energy Accelerator Research Organisation* (KEK) in Japan. Electrons are accelerated to an energy of 8 GeV, positrons to an energy of 3.5 GeV. To reach this asymmetry the electron and positron beams have their own dedicated storage ring. These rings are called *High Energy Ring* for electrons and *Low Energy Ring* and have a circumference of 3 km each. They cross each other only once at the interaction point in the *Tsukaba* area with a small ($\pm 11\,mrad$) crossing angle. Bunches with a length of 4 mm collide with a frequency of 508.887 MHz. With this setup the KEKB reached a world record luminosity of 4.49×10^{33} cm^{-2} s^{-1}.

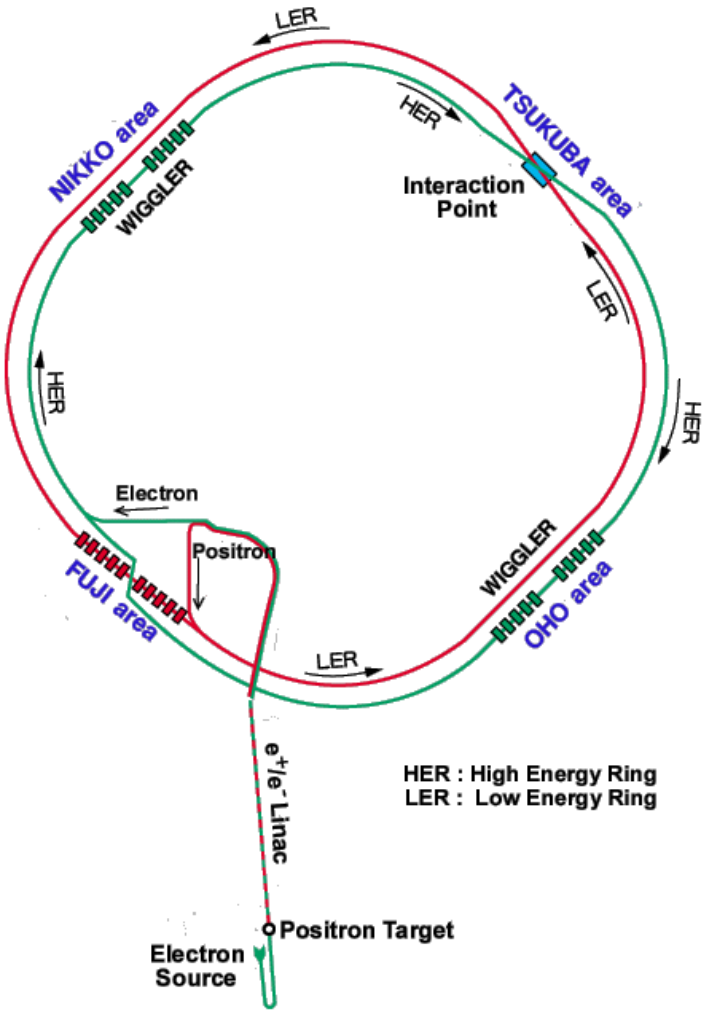

Figure 2.1: KEKB Accelerator [14]

2.3 BELLE Detector

The BELLE detector is located at the single interaction point of KEKB. Its z-axis is oriented in the opposite direction of the e^+ beam, which due to the finite crossing angle is not exactly the direction of the e^- beam. The x-axis is then set horizontally and the y-axis vertically with respect to the plane defined by the geometry of the accelerator. The BELLE detector consists of many different subdetectors, as can be seen in Fig. 2.2 I will give a short description of the subdetectors relevant to this study. A technical description can be found in Ref. [12]

- *Silicon Vertex Detector* (SVD):
  The SVD is the innermost part of the detector. Tracks of charged particles and therefore their momentum can be reconstructed very accurately in the SVD. It received a major upgrade in 2003 in which the angular coverage was upgraded from $23^\circ < \theta < 140^\circ$ to $17^\circ < \theta < 150^\circ$, matching the full angular acceptance of the BELLE detector. Its resolution σ_r in $r-\phi$ and σ_Z in $r-Z$ was measured to be

$$\sigma_r = \sqrt{21.9^2 + \left(\frac{35.5}{p}\right)^2}\,\mu m$$

$$\sigma_Z = \sqrt{27.8^2 + \left(\frac{31.9}{p}\right)^2}\,\mu m$$

  where p denotes the particle's momentum in GeV/c. This means, that the SVD alone does not yield good results for very slow particles.

- *Central Drift Chamber* (CDC):
  The central drift chamber also has an angular coverage of $17^\circ < \theta < 150^\circ$ and is filled with a gas mixture of 50% He and 50% C_2H_6. The CDC reconstructs charged particle tracks by measuring hit coordinates in the detector. This allows the reconstruction of the particle's momentum. It also measures dE/dx within its gas volume which provides additional information for the particle identification.

- *Aerogel Cherenkov counters* (ACC):
  The ACC consists of ten types of aerogel modules with refractive indices between 1.010 and 1.030. With photomultiplier tubes Cherenkov light can be detected and the particle's speed approximated. This information is also important to identify particles.

- *Time-of-flight system* (TOF):
  Using the beam collision time the TOF calculates the time it took a charged particle whose track was reconstructed by the CDC to reach the TOF. Its time resolution has

been measured to be 110 ps. ACC, TOF and CDC measurements of dE/dx provide all the information for the particle identification.

- *Electromagnetic Calorimeter* (ECL) or (CsI):
  The ECL consists of 8736 CsI(TI) crystals. Particles hitting the crystals produce scintillation light which can be detected with silicon photodiodes. Energy resolution ranges from 4% at 100 MeV to 1.6% at 8 GeV. An angular resolution between 3 mrad at high energies and 13 mrad at low energies can be achieved.

- *K_L and Muon detector* (KLM):
  The muon detector covers angles $20^\circ < \theta < 155^\circ$ and identifies muons and K_L mesons above 600 MeV/c with high efficiency. It is using alternating layers of detectors and iron plates.

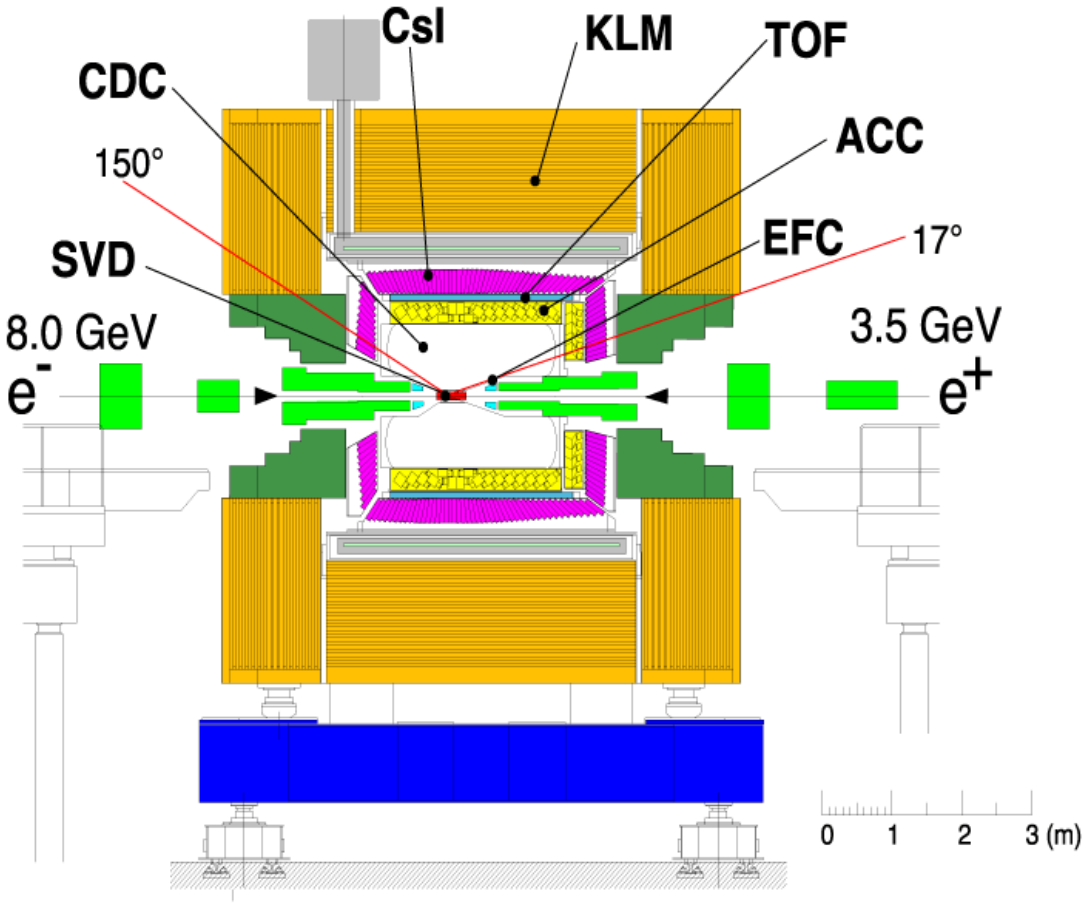

Figure 2.2: BELLE Detector [15]

Chapter 3

Method of the analysis

3.1 Decay channel and kinematics

For our analysis we chose the decay channel $\left(\Upsilon(4\mathrm{S}) \to \mathrm{B}^0\overline{\mathrm{B}}^0\right)$ with $\left(\overline{\mathrm{B}}^0 \to \mathrm{D}^{*+}\ell^-\bar{\nu}\right)$, and $\left(\mathrm{D}^{*+} \to \mathrm{D}^0\pi^+\right)$. Charge conjugated decays are always implied in this thesis. We chose this decay channel because we expect it to yield high efficiencies due to its relatively high branching fractions (Table 3.1) and the slow pion from the $\left(\mathrm{D}^{*+} \to \mathrm{D}^0\pi^+\right)$ decay. The $\Upsilon(4\mathrm{S})$ is produced by electrons with an energy of 8 GeV and positrons with an energy of 3.5 GeV, which results in a center of mass energy $\sqrt{s} = \sqrt{4E_{\mathrm{e}^-}E_{\mathrm{e}^+}} =$ 10.583 GeV. This is barely above the $\Upsilon(4\mathrm{S})$ mass of 10.579.4 GeV which is therefore emitted nearly at rest in the center-of-mass frame. The B-mesons in the decay $\Upsilon(4\mathrm{S}) \to \mathrm{B}\overline{\mathrm{B}}$ have a combined mass of $2M_{\mathrm{B}} = 10.55926$ GeV which means that the B-mesons are also emitted nearly at rest ($\beta = 0.06$, s. Chapt. 1). The decay $\overline{\mathrm{B}} \to \mathrm{D}^{*+}\ell\bar{\nu}_\ell$ is a three body decay and therefore it is impossible to predict its exact kinematics. Using only energy and momentum conservation, one can calculate the maximum energy a particle can have in the three-body decay $P_i \to P_{f1}P_{f2}P_{f3}$ [11]:

Decay channel	Branching fraction
$\Upsilon(4\mathrm{S}) \to \mathrm{B}^0\overline{\mathrm{B}}^0$	$(48.6 \pm 0.6)\%$
$\overline{\mathrm{B}}^0 \to \mathrm{D}^*\ell^-\bar{\nu}_\ell$	$(4.93 \pm 0.11)\%$
$\mathrm{D}^* \to \mathrm{D}^0\pi^+$	$(67.7 \pm 0.5)\%$

Figure 3.1: Branching fractions [5]

$$E_{f1}^{max} = \frac{m_i^2 + m_{f1}^2 - \left(m_{f2} + m_{f3}\right)^2}{2m_i} \tag{3.1}$$

Using Eq. 3.1 and the masses of all three particles, their maximum energy, momentum, and velocity can be calculated:

	M/GeV	E^{max}/GeV	p^{max}/GeV	β^{max}	γ^{max}
D^*	2.01026	3.023	2.257	0.747	1.504
ℓ	$511 \cdot 10^{-6}$	2.257	2.257	1	4417
$\bar{\nu}$	0	2.257	2.257	1	-

Table 3.1: Kinematic variables for the decay $\overline{B} \to D^* \ell \bar{\nu}$

3.2 Single-tag and Double-tag

For the following analysis the terms *single-tag* and *double-tag* have to be defined. A single-tag event is an event where one B-meson has been correctly reconstructed via the chosen decay channel and the other B-meson decayed generically. A double-tag event is an event, where both B-mesons have been correctly reconstructed via the chosen decay channel.

The number of single-tag N_s and double-tag N_d events can be calculated as follows:

$$N_s = 2N_{B\overline{B}} f_{00} \varepsilon_s \mathcal{B}\left(\overline{B} \to D^{*+} \ell^- \bar{\nu}_\ell\right) \tag{3.2}$$

$$N_d = N_{B\overline{B}} f_{00} \varepsilon_d \left[\mathcal{B}\left(\overline{B} \to D^{*+} \ell^- \bar{\nu}_\ell\right)\right]^2 \tag{3.3}$$

Where $N_{B\overline{B}}$ is the number of $B\,\overline{B}$ events in our sample, ε_s and ε_d are the reconstruction efficiencies to reconstruct a single- or double-tag event and $\mathcal{B}\left(\overline{B} \to D^{*+} \ell^- \bar{\nu}_\ell\right)$ is the branching ratio for $\overline{B} \to D^{*+} \ell^- \bar{\nu}_\ell$. Dividing Eq. 3.2 squared by Eq. 3.3 cancels out the branching ratio $\mathcal{B}\left(\overline{B} \to D^{*+} \ell^- \bar{\nu}_\ell\right)$:

$$\frac{N_s^2}{N_d} = \frac{4N_{B\overline{B}}^2 f_{00}^2 \varepsilon_s^2 \left[\mathcal{B}\left(\overline{B} \to D^{*+} \ell^- \bar{\nu}_\ell\right)\right]^2}{N_{B\overline{B}} f_{00} \varepsilon_d \left[\mathcal{B}\left(\overline{B} \to D^{*+} \ell^- \bar{\nu}_\ell\right)\right]^2} = \frac{4N_{B\overline{B}} f_{00} \varepsilon_s^2}{\varepsilon_d} \tag{3.4}$$

This leads to:

$$f_{00} = \frac{N_s^2 \varepsilon_d}{4N_d N_{B\overline{B}} \varepsilon_s^2} \tag{3.5}$$

single-tag

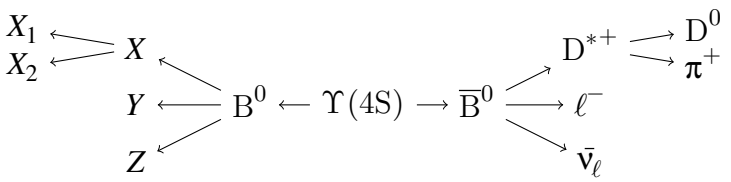

Figure 3.2: single-tag event

double-tag:

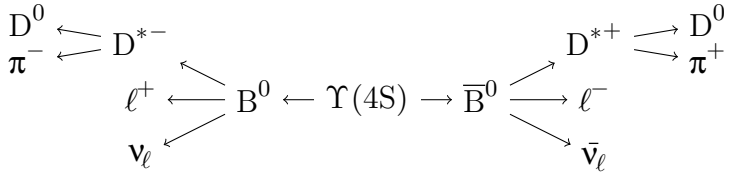

Figure 3.3: double-tag event

This equation is going to be used to determine the branching ratio

Chapter 4

Analysis

4.1 Analysis of Monte Carlo data

The first step in this bachelor thesis was the analysis of Monte Carlo signal and background. 10000 single and double-tag events, as well as 302094 background events (Table 4.1) were generated with evtgen. The particles' interaction with detector components were simulated with geant4 and they were converted to the BELLE II format. These events have been reconstructed with the BELLE II analysis software basf2.

4.1.1 Types of background

Four different types of background are to be expected:

- *mixed background* $\mathrm{e^-e^+ \to \Upsilon(4S) \to B^0\overline{B}^0}$
  Generic decays of neutral B-mesons lead to various combinations of leptons and pions which then are falsely reconstructed as signal. This will also be called combinatorial background. For double-tag events also a *semi combinatorial background* can be expected, where one side is combinatorial background and the second one is correctly reconstructed. The name mixed background derives from $\mathrm{B\ \overline{B}}$- mixing [16].
- *charged background* $\mathrm{e^-e^+ \to \Upsilon(4S) \to B^+B^-}$
  Generic decays of charged B-mesons will also produce leptons and pions that can be falsely reconstructed as signal.
- *charm background* $\mathrm{e^-e^+ \to c\overline{c}}$
  Events in which no $\mathrm{\Upsilon(4S)}$ but a $\mathrm{c\ \overline{c}}$ state is created will be called charm background.
- *uds background* $\mathrm{e^-e^+ \to q\bar{q}}$ with $q = (\mathrm{u, d, s})$
  Events that produce other quarkonium states will be summarized as uds background.

type	single-tag	double-tag	uds	charm	charged	mixed	total background
quantity	10000	10000	136139	87633	39170	39152	302094

Table 4.1: Number of signal and background events

4.1.2 Reconstruction

B-mesons were reconstructed via the decay $\overline{\mathrm{B}}^0 \to \mathrm{D}^{*+}\ell^-\bar{\nu}_\ell$ with $\mathrm{D}^{*+} \to \mathrm{D}^0\pi^+$ where only the lepton ($\ell^- = \mathrm{e}^-, \mu^-$) and the charged soft pion are reconstructed. This method leads to a much higher efficiency than reconstructing the D^0 but a priori yields no correct information about the kinematics of the reconstructed D^{*+}. Lepton candidates were required to have a center-of-mass momentum between 1.5 GeV and 2.5 GeV. The lower limit intends to suppress leptons from *charm* or *uds* background, the upper limit is due to kinematic reasons and could have been set slightly lower (Table 3.1). Pions were required to have a momentum between 60 MeV and 200 MeV in the center-of-mass frame and a momentum in z-direction between 0 MeV and 200 MeV in the lab-frame. The lower limit in the center-of-mass frame was set due to poor detector resolution for very low momenta (Sec. 2.3). Assuming both the B-meson and π^+ are emitted at rest, the pions maximum speed would be $\beta^{max} = 0.747$ (Table 3.1) which leads to a maximum momentum of $p^{max} = \beta^{max}\gamma^{max}m_{\pi^+} = 156.8$ MeV. The momentum cut in the lab frame will be explained later in Sec. 4.1.4.

The pion candidates are then used to reconstruct the D^{*+}-mesons which then are used together with the leptons to reconstruct the B-mesons. Basf2 has a built-in truth check, that verifies that a particle is correctly reconstructed. This truth check does not work here because the D^0 is missing. A different truth check is required. We can use the Monte Carlo information to verify that the B-meson really is a B-meson, that its first daughter is a lepton, its second daughter a D^{*+}-meson and its granddaughter a pion. If a reconstructed decay fulfills these four conditions it is considered as correctly reconstructed. All reconstructed B-mesons are copied in one single candidate list, which is used to reconstruct $\Upsilon(4\mathrm{S})$-mesons. Here it is important to note that due to $\mathrm{B}\ \overline{\mathrm{B}}$- mixing, it is possible to reconstruct a $\Upsilon(4\mathrm{S})$ not only from a B and a $\overline{\mathrm{B}}$, but also from two B or two $\overline{\mathrm{B}}$. Both possibilities are accounted for and the resulting lists merged into one. Events where a $\Upsilon(4\mathrm{S})$ is successfully reconstructed are saved as double-tag events, events with only one B meson are saved as single-tag events, remaining events are discarded. The leptons and pions are saved as daughter particles.

4.1.3 Reconstruction efficiency

To calculate the expected reconstruction efficiency Maryam Salehi generated a larger Monte Carlo signal sample. This sample includes a total of 200000 single-tag and 200000

double-tag events. After the reconstruction, 59558 B mesons have been saved in the single-tag output and 10041 $\Upsilon(4\mathrm{S})$ mesons have been saved as double-tag events. This also includes events, that have been falsely reconstructed so the truth check mentioned in Sec. 4.1.2 is required. After this cut is applied 20942 correctly reconstructed single-tag events and 1321 correctly reconstructed double-tag events (corresponding to 2642 correctly reconstructed B mesons) remain. This results in reconstruction efficiencies (using $\sqrt{N}$ as statistical uncertainty):

$$\varepsilon_s = \frac{20942}{200000} = (10.471 \pm 0.072)\% \tag{4.1a}$$

$$\varepsilon_d = \frac{2642}{200000} = (1.321 \pm 0.026)\%. \tag{4.1b}$$

If the efficiencies for detecting each B meson were uncorrelated the fraction $\frac{\varepsilon_d}{\varepsilon_s^2} = 1.2048$ would be equal to unity. Further work needs to be done to explain this deviation, but it is worth mentioning, that the same deviation can be found in Michael Binder's bachelor thesis [17].

4.1.4 D^{*+} momentum

Without reconstructing the D^0 we can't reconstruct the momentum of the D^{*+}. However, the D^{*+}mass is only slightly above the combined mass of the D^0 and π^+ which means, that the π^+ will be very slow in the D^{*+}frame. Therefore we can approximate the D^{*+}momentum as linear function of the π^+ momentum. This can be seen in Figs. 4.1 - 4.6. Scatter plots create an entry for every event and show a considerable spread. This spread originates from the fact that the π^+ is not emitted completely at rest in the D^{*+}frame. Profile plots average all entries for each bin on the x-axis (blue) and are used to perform the linear fit (red). The fit parameters can be found in Table A.1 in the appendix.

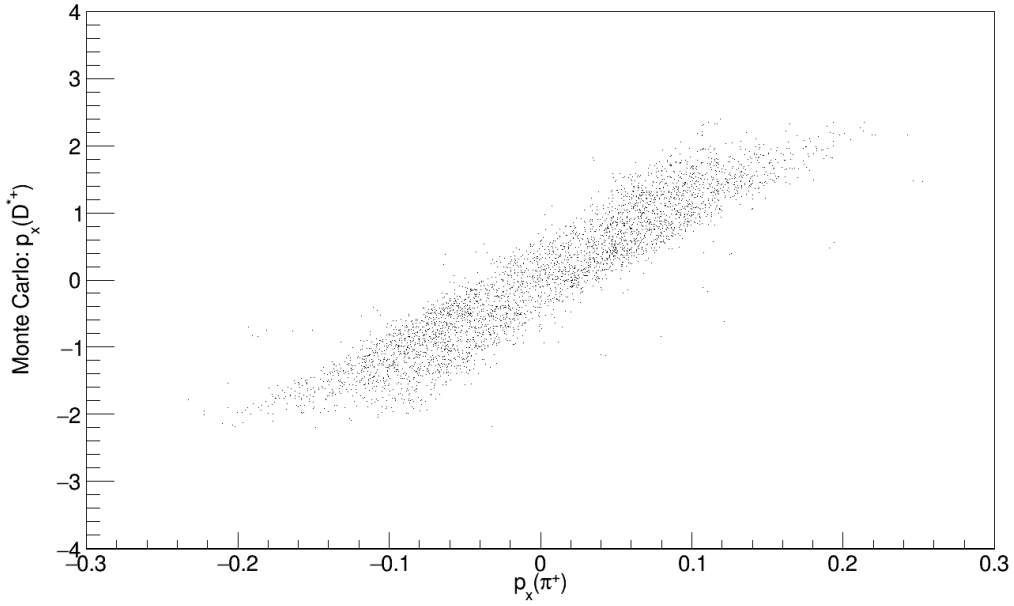

Figure 4.1: Scatter plot: Relation between measured π^+ momentum and Monte Carlo D^{*+}momentum in x-direction

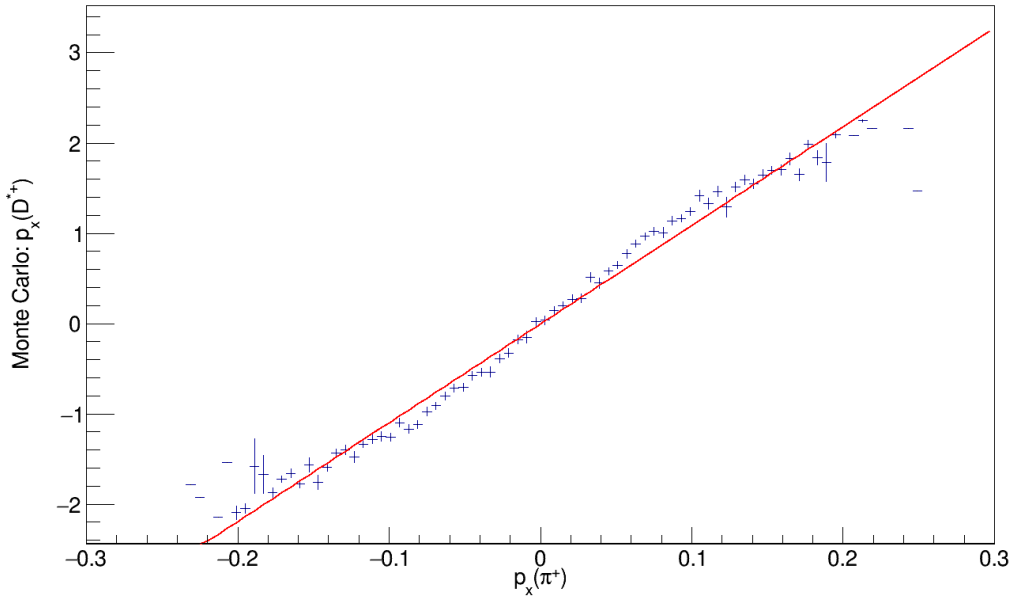

Figure 4.2: Profile plot: Relation between measured π^+ momentum and Monte Carlo D^{*+}momentum in x-direction

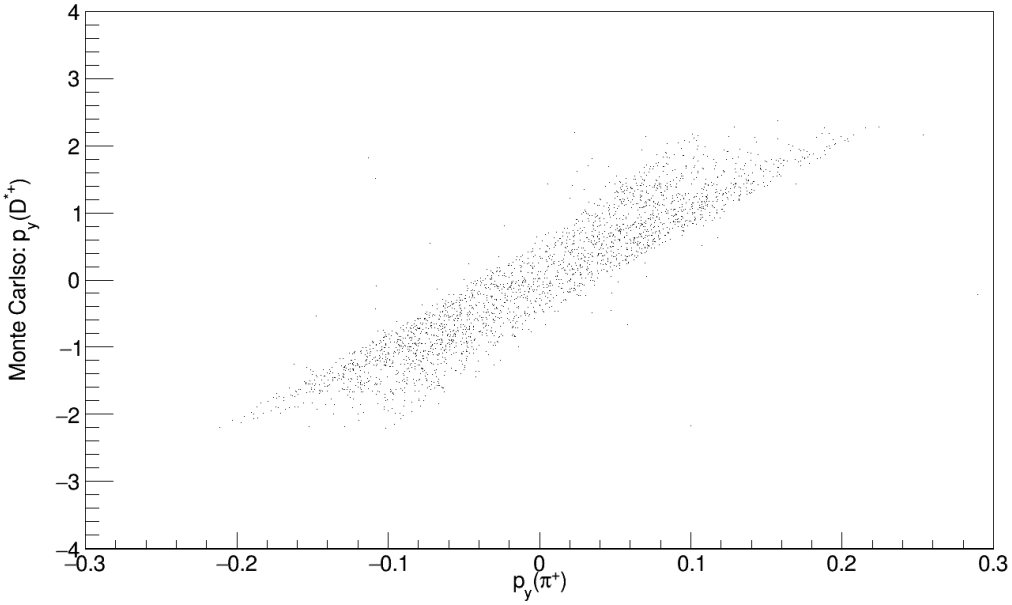

Figure 4.3: Scatter plot: Relation between measured π^+ momentum and Monte Carlo D^{*+}momentum in y-direction

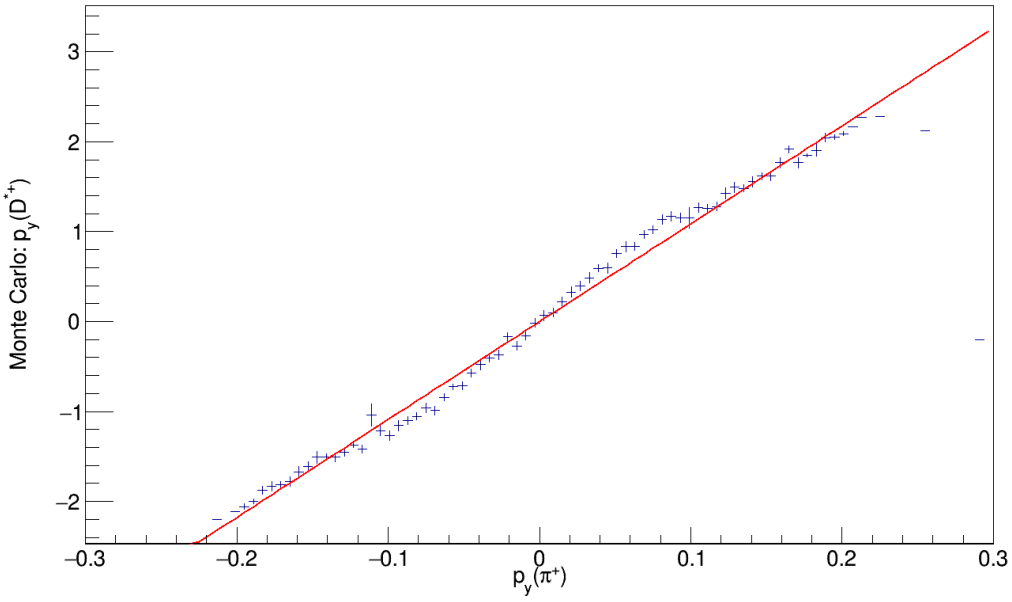

Figure 4.4: Profile plot: Relation between measured π^+ momentum and Monte Carlo D^{*+}momentum in y-direction

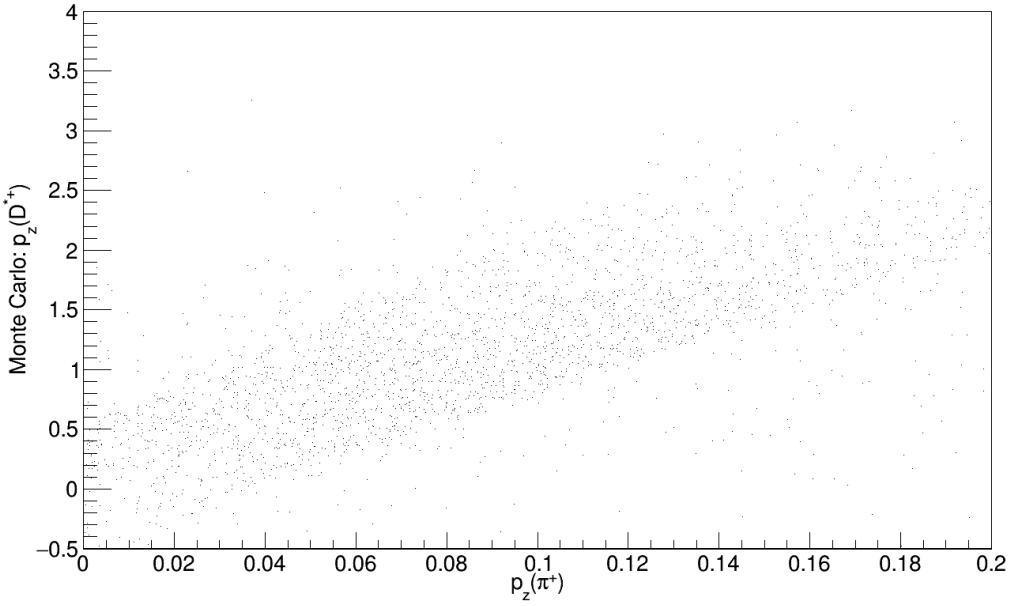

Figure 4.5: Scatter plot: Relation between measured π^+ momentum and Monte Carlo D^{*+}momentum in z-direction

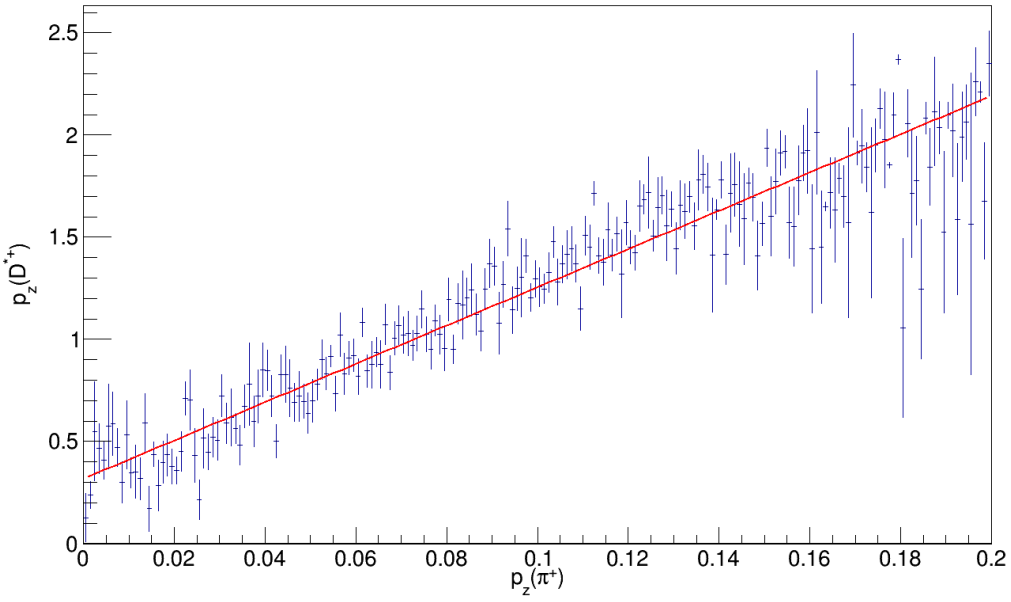

Figure 4.6: Profile plot: Relation between measured π^+ momentum and Monte Carlo D^{*+}momentum in z-direction

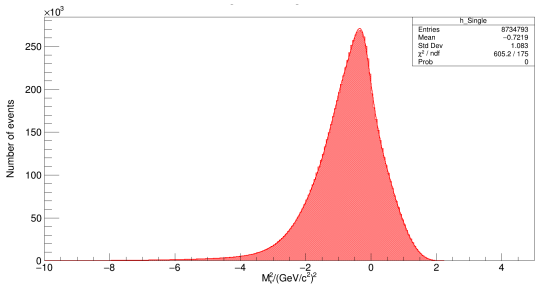

Figure 4.7: Monte Carlo data, signal: single-tag events

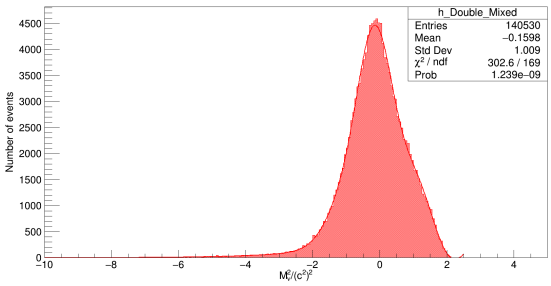

Figure 4.8: Monte Carlo data, signal: double-tag events

4.1.5 Fit variable

A variable is needed to separate signal from background. For this the squared, invariant neutrino mass $\mathcal{M}_\nu^2$ shall be used. It can be calculated in the center-of-mass frame of the $\Upsilon(4S)$ which is assumed to be the center-of-mass frame of the B as follows:

$$\begin{aligned} \mathcal{M} &= E_\nu^2 - \mathbf{p}_\nu^2 = \\ &= \left(E_{beam} - E_{D^{*+}} - E_\ell\right)^2 - \left(\mathbf{p}_{D^{*+}} + \mathbf{p}_\ell\right)^2 \end{aligned} \tag{4.2}$$

This variable is calculated with the approximation from Sec. 4.1.4 for each event using ROOT. Plotted as a histogram and fitted using a combination of seven Gaussian functions. If an event is correctly reconstructed, the missing neutrino mass should be 0, otherwise Eq. 4.2 does not describe the missing neutrino mass or any other physical quantity. To perform these fits, a larger data set was required. We used Monte Carlo data containing all four different kinds of background where our signal is part of the mixed background. This sample contained $(619.620 \pm 9.441) \cdot 10^6$ B $\overline{\text{B}}$ events. Figs. 4.7 - 4.17 show the resulting distributions for single- and double-tag events. The fit parameters can be looked up in the Tables A.2 and A.3.

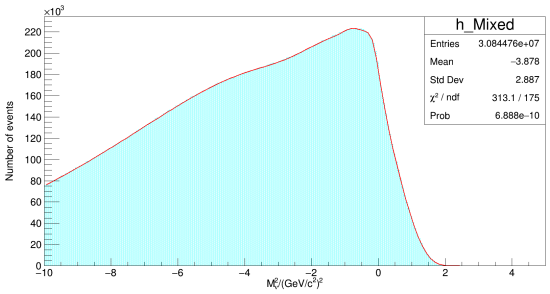

Figure 4.9: Monte Carlo data, mixed background: single-tag events

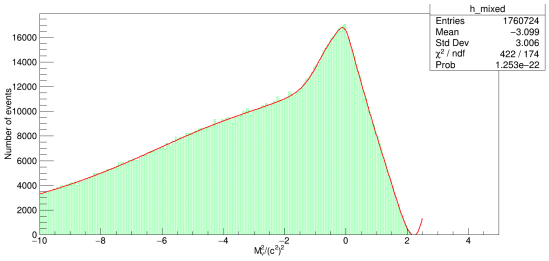

Figure 4.10: Monte Carlo data, mixed background: double-tag events

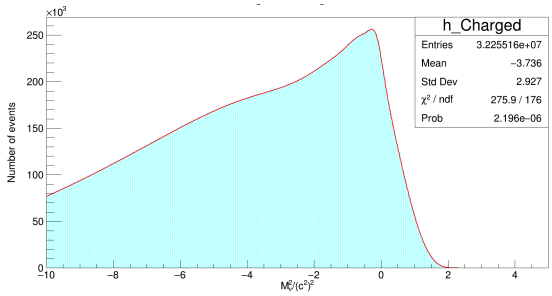

Figure 4.11: Monte Carlo data, charged background: single-tag events

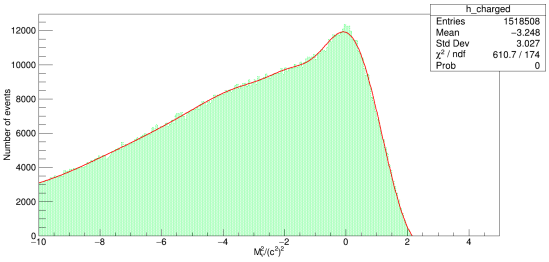

Figure 4.12: Monte Carlo data, charged background: double-tag events

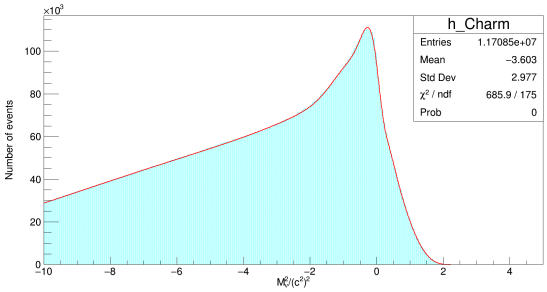

Figure 4.13: Monte Carlo data, Charm background: single-tag events

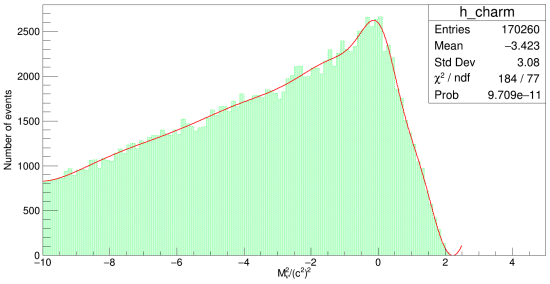

Figure 4.14: Monte Carlo data, Charm background: double-tag events

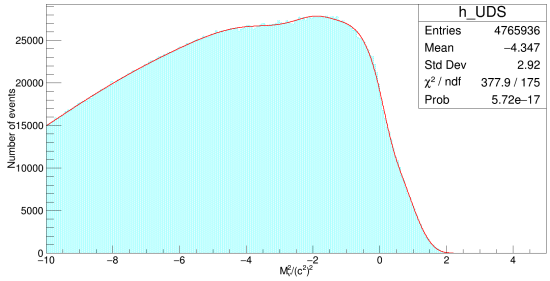

Figure 4.15: Monte Carlo data, Uds background: single-tag events

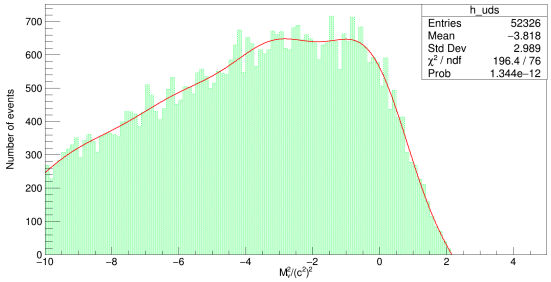

Figure 4.16: Monte Carlo data, Uds background: double-tag events

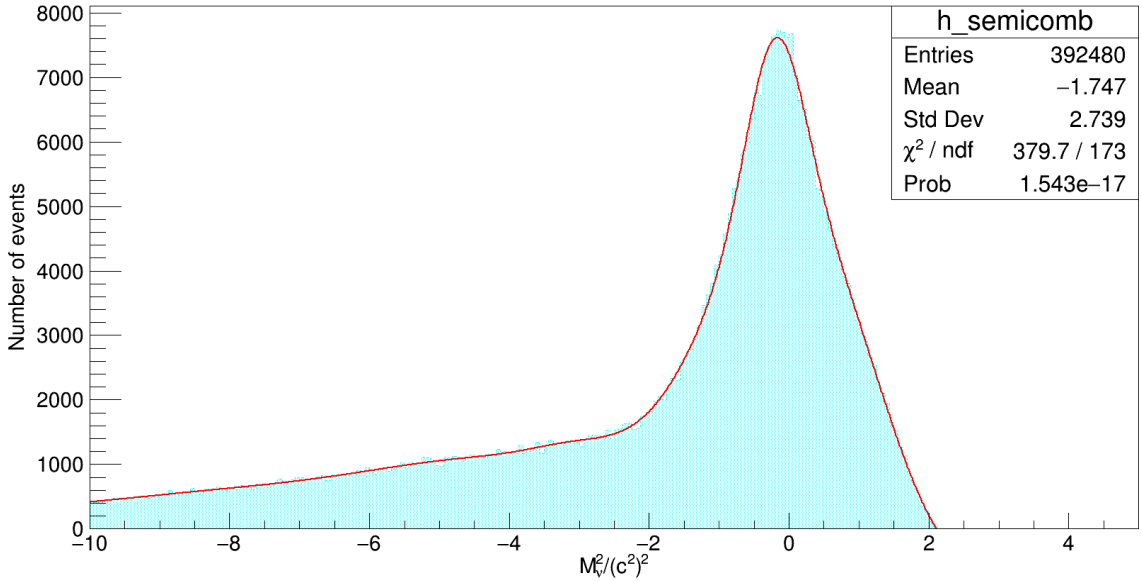

Figure 4.17: Monte Carlo data, semi combinatorial background: double-tag events

4.2 Analysis of BELLE data

The same reconstruction as on Monte Carlo data has been performed on experiment 41 of the BELLE data set. This data set includes $N_{\mathrm{B\overline{B}}} = 64.0134^{+0.9863}_{-0.9857} \cdot 10^6$ B $\overline{\mathrm{B}}$ events [13]. The $\mathcal{M}_{\nu}^2$ distribution has been plotted and fitted for both single-tag and double-tag events (Figs. 4.18 and 4.19). The functions used to fit the distributions were the sums of all fit functions obtained from Monte Carlo data with fixed parameters and one free scaling coefficient for each function (Eq. 4.3) . The free parameters were then determined by the fit in ROOT.

$$\text{single-tag:} \qquad f_{fit} = p_0^S f_{signal} + p_1^S f_{mixed} + p_2^S f_{charged} + p_3^S f_{charm} + p_4^S f_{uds} \tag{4.3a}$$

$$\text{double-tag:} \qquad g_{fit} = p_0^D g_{signal} + p_1^D g_{semi} + p_2^D g_{mixed} + p_3^D g_{charged} + p_3^D g_{charm} + p_4^D g_{uds} \tag{4.3b}$$

The number of signal or background events can be calculated as the number of events in the original fit function multiplied with the value of its free coefficient. This does not work properly with mixed and charged background. Their shapes (Figs. 4.9 and 4.11) are very similar and thus their free coefficients are anti-correlated. Since the signal distribution (Fig. 4.7) differs strongly from all background distributions it should yield good results for the number of single-tag and double-tag events. Using the fit parameters from Figs. 4.18 and 4.19 as well as the number of Monte Carlo signals from Figs. 4.7 and 4.8 N_s and N_d are calculated with the statistical error obtained from the uncertainty on the scaling coefficient $p0$.

$$N_s = (0.2169 \pm 0.0025) \cdot 8.734793 \cdot 10^6 = (1.8946 \pm 0.0218) \cdot 10^6 \tag{4.4a}$$

$$N_d = (0.2569 \pm 0.0132) \cdot 1.40530 \cdot 10^5 \ = (3.6102 \pm 0.1855) \cdot 10^4 \tag{4.4b}$$

f_{00} can now be calculated with Eq. 3.5:

$$f_{00} = \frac{\varepsilon_d}{\varepsilon_s^2} \frac{N_s^2}{4 N_d N_{\mathrm{B\overline{B}}}} = 0.46783 \tag{4.5}$$

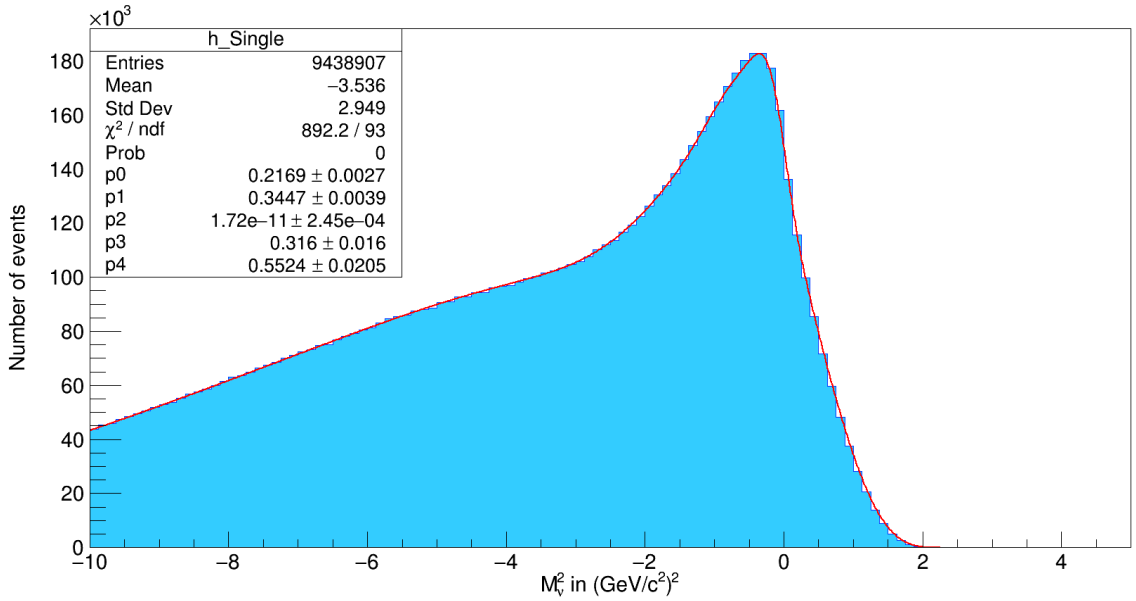

Figure 4.18: single-tag events

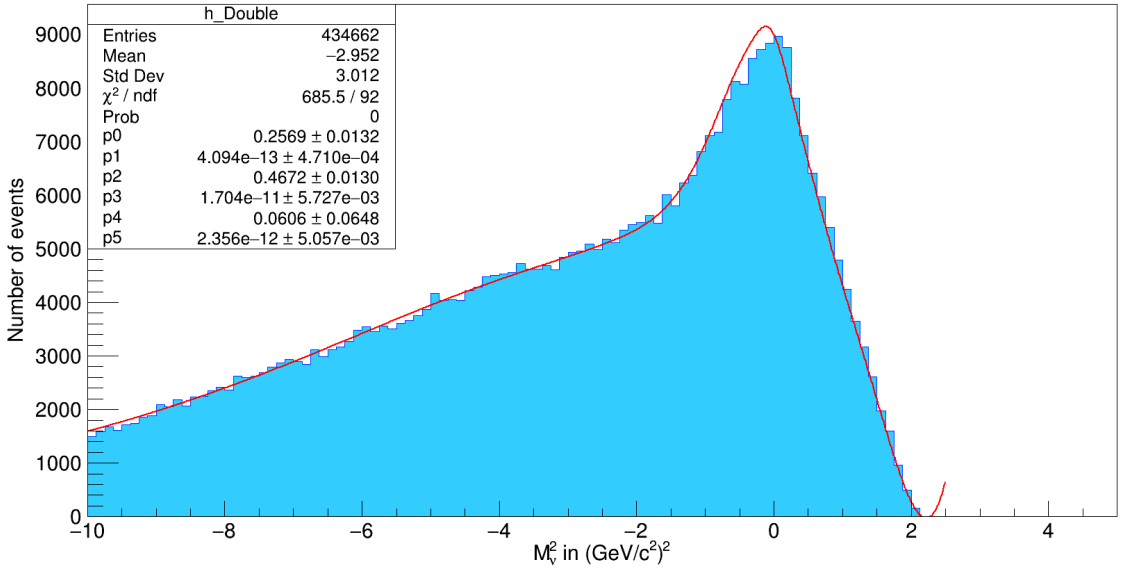

Figure 4.19: double-tag events

4.3 Uncertainty

4.3.1 Statistical Uncertainty

The statistical uncertainty comes from the uncertainty on the reconstruction efficiencies ε_s and ε_d, and the uncertainty on the number of events $N_{\mathrm{B}\overline{\mathrm{B}}}$, N_s and N_d. Using a Gaussian propagation of uncertainty the statistical error ε_s can be calculated.

$$\begin{aligned}\sigma_s &= \sqrt{\left(\frac{\partial f_{00}}{\partial \varepsilon_s}\sigma_{\varepsilon_s}\right)^2 + \left(\frac{\partial f_{00}}{\partial \varepsilon_d}\sigma_{\varepsilon_d}\right)^2 + \left(\frac{\partial f_{00}}{\partial N_s}\sigma_{N_s}\right)^2 + \left(\frac{\partial f_{00}}{\partial N_d}\sigma_{N_d}\right)^2 + \left(\frac{\partial f_{00}}{\partial N_{\mathrm{B}\overline{\mathrm{B}}}}\sigma_{N_{\mathrm{B}\overline{\mathrm{B}}}}\right)^2} \\ &= \sqrt{4.140\cdot 10^{-5} + 8.479\cdot 10^{-5} + 1.160\cdot 10^{-4} + 5.779\cdot 10^{-4} + 5.193\cdot 10^{-5}} \\ &= 2.953\cdot 10^{-2}\end{aligned} \tag{4.6}$$

Therefore the result of this bachelor's thesis is

$$f_{00} = (46.783 \pm 2.953)\% \tag{4.7}$$

4.3.2 Systematic Uncertainty

Estimating the systematic uncertainty on this analysis is a complicated and time consuming task that exceeds the amount of work which can be put in this bachelor's thesis. Possible systematic errors can originate from:

- a difference between simulated Monte Carlo data and experimental data
- limited accuracy and resolution in the BELLE detector
- the assumption that B mesons are emitted at rest
- errors in the linear correlation made in section 4.1.4
- uncertainties on the fits made in on Monte Carlo data.

Chapter 5

Outlook

The result obtained in this bachelor's thesis is consistent with previous measurements, but its accuracy does not yet match that of the measurements by the BABAR collaboration [2]. Further work can be done to improve this analysis. The main contribution to the statistical error is the uncertainty on N_s and N_d. By using a larger data sample or even the full BELLE data set their share could be decreased. Using more sophisticated fit functions can also reduce the error on N_s and N_d. The uncertainties on ε_s, ε_d and $N_{\mathrm{B\overline{B}}}$ have not been negligible in this study either. While improving the accuracy on $N_{\mathrm{B\overline{B}}}$ seems very difficult, measurements of ε_s and ε_d can be improved by using more simulated Monte Carlo data. The reconstruction efficiencies can also be increased by tweaking the steering file used for the reconstruction. As mentioned in Sec. 4.1.2 some cuts could have been changed but remained to stay consistent throughout the analysis. Removing the cut on the pion momentum in z-direction would double the reconstruction efficiency, but also have negative effects on the approximation of the D^{*+}momentum (Sec. 4.1.4). Future work could reevaluate the necessity of this cut. We also have not provided an answer why the reconstruction efficiencies ε_s and ε_d seem to be correlated in our analysis. Most importantly though systematic uncertainties have to be estimated.

Appendix A

Appendix

	$p0$	$\Delta p0$	$p1$	$\Delta p1$
x-direction	0.0031	0.0070	10.65	0.0604
y-direction	0.0021	0.0062	10.78	0.0470
z-direction	0.2650	0.0146	10.20	0.1593

Table A.1: Fit parameters for linear fit

Table A.2: Fit parameters (Singletag)

Singletag: Signal						
	constant	error	mean	error	sigma	error
Gaussian 1	-3.17861e+05	2.73172e+01	9.20308e-01	8.42673e-05	-1.06068e+00	6.99178e-05
Gaussian 2	3.12409e+04	1.59635e+01	3.41943e+00	5.28166e-03	-3.67066e+00	3.32772e-03
Gaussian 3	7.34627e+04	1.21960e+04	3.66788e+07	4.23908e+05	9.68360e+06	1.11881e+05
Gaussian 4	3.78194e+05	3.44165e+01	4.07503e-01	9.36483e-05	1.28370e+00	6.82429e-05
Gaussian 5	5.00276e+04	5.93320e+02	-6.06879e-01	4.88678e-03	-4.21303e-01	2.25368e-03
Gaussian 6	5.27083e+04	7.27928e+02	-2.58447e-01	1.98881e-03	-2.28318e-01	2.18845e-03
Gaussian 7	-1.45634e+05	1.09994e+02	5.64944e+00	6.54094e-04	1.70381e+00	3.29647e-04
Singletag: Mixed background						
Gaussian 1	1.61173e+06	5.03994e+01	-4.99829e+00	9.40123e-05	4.36202e+00	5.98176e-05
Gaussian 2	-1.44502e+06	5.27701e+01	-5.19459e+00	1.10764e-04	4.23853e+00	6.80409e-05
Gaussian 3	5.80424e+04	3.23550e+02	-7.54304e-01	2.47539e-03	1.05117e+00	1.61291e-03
Gaussian 4	3.41053e+04	5.12323e+02	-3.84552e-01	4.93804e-03	4.66324e-01	4.87641e-03
Gaussian 5	-2.38919e+04	4.15131e+01	1.34929e+00	7.10254e-04	5.72482e-01	4.95240e-04
Gaussian 6	1.88494e+04	5.25277e+02	-1.61024e-01	3.81698e-03	1.83125e-01	5.06985e-03
Gaussian 7	-9.20298e+04	1.59003e+01	1.90474e+00	1.42448e-03	1.75007e+00	4.82514e-03
Singletag: Charged background						
Gaussian 1	1.61355e+06	2.22573e+01	-4.84569e+00	1.15865e-04	4.42035e+00	1.37956e-04
Gaussian 2	-1.44426e+06	3.35837e+01	-5.04312e+00	1.27329e-04	4.28926e+00	1.17206e-04
Gaussian 3	7.19961e+04	1.06136e+03	-4.79207e-01	4.10789e-03	1.08825e+00	2.13727e-03
Gaussian 4	3.42520e+04	7.80512e+02	-3.34240e-01	7.04773e-03	4.48546e-01	5.57199e-03
Gaussian 5	-4.53840e+04	1.27008e+02	1.29935e+00	8.40561e-04	6.46839e-01	1.39248e-03
Gaussian 6	2.40451e+04	8.10410e+02	-1.40995e-01	3.38592e-03	1.80998e-01	5.49742e-03
Gaussian 7	-9.22997e+04	2.25363e+01	2.29160e+00	1.04011e-02	1.74096e+00	1.72861e-02
Singletag: Charm background						
Gaussian 1	1.64194e+06	2.93398e+00	5.41364e+00	3.20635e-05	7.14453e+00	4.82700e-05
Gaussian 2	-1.42650e+06	2.86631e+00	4.48345e+00	4.49863e-05	6.63214e+00	1.25764e-04
Gaussian 3	2.37781e+04	3.38472e+02	-4.55278e-01	4.63440e-03	6.70462e-01	4.24220e-03
Gaussian 4	-9.05683e+03	3.27982e+02	1.72729e-01	4.64811e-03	-1.52527e-01	5.20347e-03
Gaussian 5	-8.74565e+04	4.75073e+00	1.60743e+00	9.50438e-05	1.15095e+00	4.20507e-04
Gaussian 6	2.57384e+04	2.24639e+02	-1.51768e-01	5.01791e-03	2.85130e-01	2.76772e-03
Gaussian 7	-4.79119e+07	1.40493e+03	1.65605e+01	3.05004e-05	3.94224e+00	8.30770e-06
Singletag: Uds background						
Gaussian 1	1.64591e+06	1.20344e+01	5.14922e+00	1.07098e-04	6.64767e+00	2.10234e-04
Gaussian 2	-1.42044e+06	1.14111e+01	4.09492e+00	1.55704e-04	6.20504e+00	2.41942e-04
Gaussian 3	-2.09712e+03	1.71980e+02	-1.18476e+00	2.39278e-02	5.46944e-01	2.87967e-02
Gaussian 4	-4.41022e+03	9.79745e+01	-2.28518e+00	3.95673e-02	-1.17178e+00	2.26851e-02
Gaussian 5	-3.56992e+04	1.21065e+01	1.44547e+00	7.44552e-04	1.28078e+00	9.99566e-04
Gaussian 6	-1.91690e+03	6.39536e+01	3.48624e-01	9.05637e-03	2.91239e-01	9.44608e-03
Gaussian 7	-2.36611e+06	2.47297e+02	1.62535e+01	2.35921e-04	5.63811e+00	9.44008e-05

Table A.3: Fit parameters (Doubletag)

Doubletag: Signal						
	constant	error	mean	error	sigma	error
Gaussian 1	-3.25030e+05	6.01912e+01	6.67414e-01	1.46739e-04	-9.38230e-01	1.06126e-04
Gaussian 2	3.47118e+02	3.39588e+00	3.37235e+02	3.14794e+00	-3.33430e+02	3.03642e+00
Gaussian 3	-8.10992e+07	7.96953e+05	8.76101e+07	3.35197e+04	1.72427e+07	6.60122e+03
Gaussian 4	3.31739e+05	6.08905e+01	6.54724e-01	1.44725e-04	9.35852e-01	1.03766e-04
Gaussian 5	-6.70582e+02	5.02613e+01	-7.30571e-01	2.85340e-02	-4.39795e-01	2.22050e-02
Gaussian 6	-4.87553e+03	7.34772e+01	5.21301e-01	5.11269e-03	5.66350e-01	4.85087e-03
Gaussian 7	1.41575e+03	5.27473e+01	6.43171e+00	1.10768e-01	3.83131e+00	4.20379e-02
Doubletag: Semicombinatorial background						
Gaussian 1	1.57284e+06	2.66701e+01	-5.09330e+00	1.03799e-04	4.23509e+00	1.02230e-04
Gaussian 2	-1.48257e+06	2.67149e+01	-5.12343e+00	1.07821e-04	4.18220e+00	1.06498e-04
Gaussian 3	2.84129e+02	1.70393e+01	-2.98955e+00	3.87049e-02	6.56181e-01	4.44604e-02
Gaussian 4	2.58629e+03	3.97950e+01	-1.98834e-01	5.77094e-03	4.04857e-01	7.13101e-03
Gaussian 5	5.54156e+04	3.93357e+01	3.04160e+01	1.92919e-02	3.02335e+01	1.66679e-02
Gaussian 6	7.48449e+03	3.84038e+01	1.99521e-01	4.64985e-03	1.29650e+00	5.71440e-03
Gaussian 7	-1.19213e+05	2.47095e+01	-3.88480e+00	2.04399e-03	6.34564e+00	2.54835e-03
Doubletag: Mixed background						
Gaussian 1	1.53272e+06	4.22821e+01	-5.12448e+00	1.05464e-04	4.20734e+00	7.25460e-05
Gaussian 2	-1.52467e+06	4.22908e+01	-5.13623e+00	1.05821e-04	4.20045e+00	7.28363e-05
Gaussian 3	6.00327e+03	1.23239e+02	-1.00823e-01	8.49790e-03	6.51197e-01	1.00524e-02
Gaussian 4	9.30717e+02	1.05708e+02	-3.62774e-02	1.72016e-02	1.87722e-01	3.32789e-02
Gaussian 5	7.20267e+05	2.49977e+02	9.53351e+00	5.18445e-04	3.31561e+00	2.33626e-04
Gaussian 6	1.21557e+05	2.11446e+01	2.24460e+00	1.03354e-03	1.15991e+00	1.71588e-03
Gaussian 7	-1.98551e+05	2.23824e+01	2.61832e+00	4.13082e-04	1.33041e+00	8.80224e-04
Doubletag: Charged background						
Gaussian 1	1.57991e+06	6.30579e+00	-3.30192e+00	1.14718e-05	3.51111e+00	7.70552e-06
Gaussian 2	-1.47519e+06	6.52142e+00	-3.36323e+00	1.24929e-05	3.46132e+00	8.21932e-06
Gaussian 3	-3.84746e+07	5.36871e+08	-1.72015e+02	1.41421e+00	4.37785e+00	1.41421e+00
Gaussian 4	9.53579e+02	2.32296e+01	-1.80313e+00	2.21392e-02	6.41150e-01	1.83543e-02
Gaussian 5	1.09063e+05	3.73219e+00	1.20443e+01	4.42070e-04	1.14961e+01	4.69816e-04
Gaussian 6	1.03318e+04	9.68452e+00	3.51309e-01	6.57111e-04	1.03944e+00	3.91436e-04
Gaussian 7	-1.57693e+05	2.88932e+00	-7.66953e-01	1.75352e-04	5.35354e+00	2.56507e-04
Doubletag: Charm background						
Gaussian 1	1.56974e+06	1.89030e+01	-5.06392e+00	3.86966e-05	4.25933e+00	2.61724e-05
Gaussian 2	-1.48557e+06	1.90444e+01	-5.07555e+00	4.08532e-05	4.20234e+00	2.75943e-05
Gaussian 3	1.76147e+03	2.35148e+01	-4.68247e-01	1.48407e-02	1.30660e+00	9.03086e-03
Gaussian 4	-1.71744e+03	4.56959e+01	7.12086e-01	9.41729e-03	5.12529e-01	7.35825e-03
Gaussian 5	6.03141e+04	7.12394e+00	2.49099e+01	2.66592e-02	7.28078e+01	7.89388e-02
Gaussian 6	3.11015e+03	4.54591e+01	6.73155e-01	5.86737e-03	7.23585e-01	3.15111e-03
Gaussian 7	-1.38315e+05	9.79311e+00	-4.58969e+00	5.98259e-04	7.59408e+00	6.88724e-04
Doubletag: Uds background						
Gaussian 1	1.57190e+06	1.59875e+02	-5.08358e+00	7.87935e-04	4.28026e+00	9.35798e-04
Gaussian 2	-1.48348e+06	1.56940e+02	-5.12286e+00	8.98353e-04	4.22361e+00	1.09838e-03
Gaussian 3	4.02914e+03	2.81362e+02	4.11009e-01	1.40565e-01	1.57767e+00	1.38113e-01
Gaussian 4	-5.31583e+02	3.99762e+02	-4.23995e+00	4.29656e-01	-1.44153e+00	2.47567e-01
Gaussian 5	3.40060e+04	3.52377e+01	1.64452e+01	4.08713e-02	2.43380e+01	1.12313e-01
Gaussian 6	6.19972e+03	2.52194e+02	2.94602e+00	7.96450e-02	1.61953e+00	1.86568e-01
Gaussian 7	-1.13415e+05	9.38504e+01	-3.60812e+00	5.46693e-03	6.47639e+00	2.90480e-02

Bibliography

[1] S. Dubynskiy, A. Le Yaouanc, L. Oliver, J.-C. Raynal and M. B. Volosin, Phys. Rev. D **75** (2007) 113001 doi:10.1103/PhysRevD.75.113001 [arXiv:0704.0293 [hep-ph]].

[2] B. Aubert *et al.* [BaBar Collaboration], Phys. Rev. Lett. **95** (2005) 042001 doi:10.1103/PhysRevLett.95.042001 [hep-ex/0504001].

[3] M. Jung, Phys. Lett. B **753** (2016) 187 doi:10.1016/j.physletb.2015.12.024 [arXiv:1510.03423 [hep-ph]].

[4] Bettini, A. 2009. *Introduction to Elementary Particle Physics*. Cambridge: Cambridge University Press, pp.98ff.

[5] C. Patrignani *et al.* [Particle Data Group], Chin. Phys. C **40** (2016) no.10, 100001. doi:10.1088/1674-1137/40/10/100001

[6] B. Aubert *et al.* [BaBar Collaboration], Phys. Rev. D **69** (2004) 071101 doi:10.1103/PhysRevD.69.071101 [hep-ex/0401028].

[7] N. C. Hastings *et al.* [Belle Collaboration], Phys. Rev. D **67** (2003) 052004 doi:10.1103/PhysRevD.67.052004 [hep-ex/0212033].

[8] S. B. Athar *et al.* [CLEO Collaboration], Phys. Rev. D **66** (2002) 052003 doi:10.1103/PhysRevD.66.052003 [hep-ex/0202033].

[9] B. Aubert *et al.* [BaBar Collaboration], Phys. Rev. D **65** (2002) 032001 doi:10.1103/PhysRevD.65.032001 [hep-ex/0107025].

[10] J. P. Alexander *et al.* [CLEO Collaboration], Phys. Rev. Lett. **86** (2001) 2737 doi:10.1103/PhysRevLett.86.2737 [hep-ex/0006002].

[11] Griffiths, D. 1996. *Einführung in die Elementarteilchenphysik*. Berlin: Akad.-Verl., pp.89ff, 115ff.

[12] Ed. A.J. Bevan, B. Golob, Th. Mannel, S. Prell, and B.D. Yabsley, Eur. Phys. J. C74 (2014) 3026, SLAC-PUB-15968, KEK Preprint 2014-3

[13] Number of recorded $\mathrm{B}\,\overline{\mathrm{B}}$ events on the BELLE webpage:
`https://belle.kek.jp/secured/nbb/nbb.html`

[14] Wikipedia article about the KEKB accelerator.
`https://upload.wikimedia.org/wikipedia/commons/c/c2/KEKB.png`
(last downloaded on 24.07.2017)

[15] A. Abashian, *et al*. [Belle Collaboration], The Belle detector, Nuclear Instruments and Methods in Physics Research Section A: Accelerators, Spectrome- ters, Detectors and Associated Equipment, Volume 479, Issue 1, 2002, Pa- ges 117-232, ISSN 0168-9002, http://dx.doi.org/10.1016/S0168-9002(01)02013-7. `http://www.sciencedirect.com/science/article/pii/S0168900201020137`

[16] *Observation of B0 - anti-B0 Mixing* - ARGUS Collaboration (Albrecht, H. et al.) Phys.Lett. B192 (1987) 245-252 DESY-87-029

[17] Binder, M. 2017 *Studien zur Bestimmung des Verzweigungsverhältnisses f_{+-} des Zerfalls* $\Upsilon(4\mathrm{S}) \rightarrow \mathrm{B}^{+}\mathrm{B}^{-}$, unpubllished

List of Figures

List of Tables

Erklärung

Hiermit erkläre ich, die vorliegende Arbeit selbständig verfasst zu haben und keine anderen als die in der Arbeit angegebenen Quellen und Hilfsmittel benutzt zu haben.

München, den ...

(Name einfügen)

Acknowledgements

I am grateful to professor Thomas Kuhr for giving me the opportunity to work on this thesis in his group and for his continous support over the last few weeks. I would also like to thank James Kahn for his numerous explanations, his help with the analysis and his constructive feedback. I also would like to thank Dr. Martin Ritter for helping me with various technical problems and Maryam Salehi for providing me with a larger Monte Carlo sample. A special thanks goes to Kasper van Schie for proof reading this thesis on very short notice. Last but not least I want to thank my fellow bachelor students Michael Binder, Vincent Eberle, Sebastian Eppelt, Jaron Grigat and Carlotta Versmold for their mutual support and for creating a pleasent atmosphere in our office.